RESEARCH ARTICLE

Jetting onset on a liquid surface accelerated past a submerged cylinder– Supplementary Material

Rubert Martín Pardo*⬮, Niloy Barua⬮, Daphné Lisak⬮ and Jovan Nedić⬮[1,1,1]

Department of Mechanical Engineering, McGill University, Montreal, QC H3A 0C3, Canada
*Corresponding author. E-mail: rubert.martin@mail.mcgill.ca

1. Description of the apparatus

The main body of the apparatus consists of a vertical cylindrical steel bore that is mounted and levelled on an aluminium extrusion structure fixed to the floor. The bore is composed of a lower and an upper section (fig. 2a and b), each containing aluminium pistons that slide freely between stops located at the ends of each section. The upper piston is referred herein as the *pusher piston* (fig. 2c) and the lower piston is called the *driver piston* (fig. 2d). The volumes on either side of a piston are isolated from one another by sealing o-rings (fig. 2e) placed on the pistons. A compressed gas reservoir (fig. 2f) is connected to the lower bore by means of a normally closed solenoid valve (fig. 2g). The top of the upper bore section connects to a 3-D printed outlet (fig. 2h), which in turn is connected to an acrylic water tank (fig. 2i). The outlet serves as a transition between the cylindrical cross-section of the bore and the
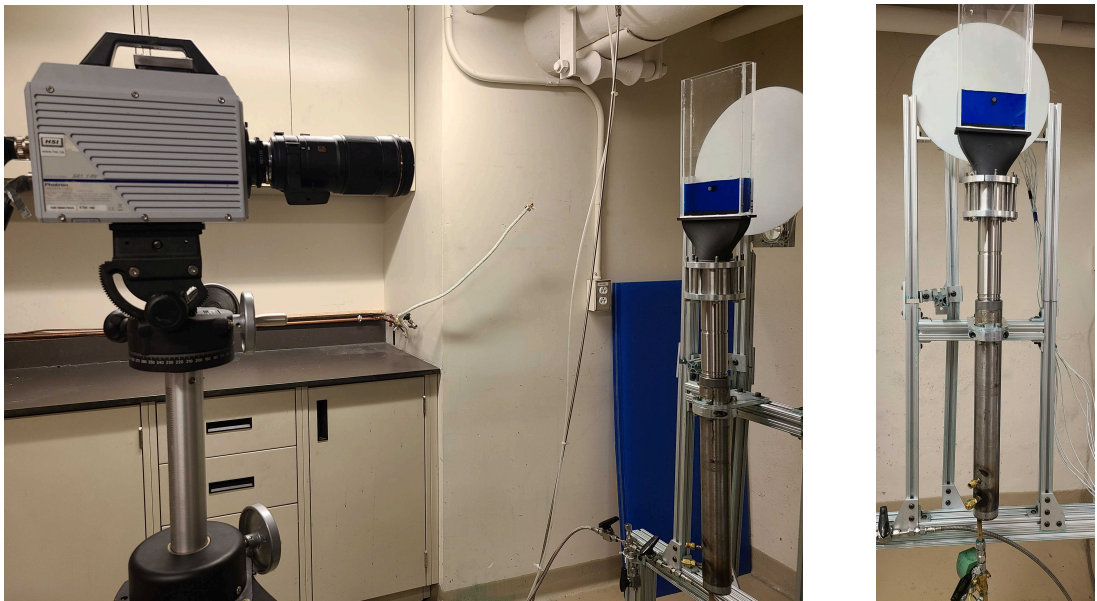

Figure 1: Experimental set-up (left): Side view including the high-speed camera. (right): Front view.

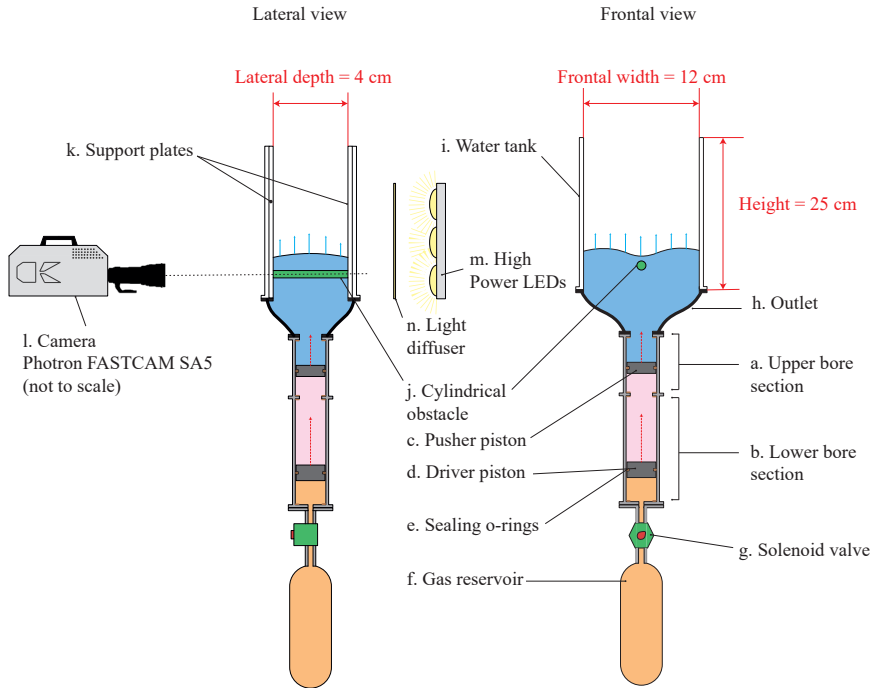rectangular cross-section of the water tank. Before each experiment, both the lower and the upper pistons

Figure 2: Diagram of the Experimental Apparatus (not to scale). Individual components are labelled in black with Latin letters. Water tank dimensions are labelled in red.

were seated on the lower ends of their corresponding bore sections. The space above the upper piston is filled with water until the desired fill height is reached in the water tank. The gas reservoir below the solenoid valve contained pressurised nitrogen gas. A minimum pressure of 3.5 MPa guarantees that the pistons will overcome any friction and move the full length of the corresponding bores. A pressure of 0.7 MPa is set as an upper limit to minimise the wear resulting from high-speed impacts between the pistons and the stops located inside the bores. The space between the two pistons was initially filled with air at atmospheric pressure. The experiment was initiated by triggering the valve to its open state allowing the compressed nitrogen to expand into the lower section of the bore causing the lower piston to accelerate, compressing the air above it and pushing the upper piston in a manner much like two bodies interconnected by a spring. This double piston setup provides an efficient way for generating high acceleration rates over a short time. A horizontal cylindrical obstacle (fig. 2j) can be placed within the water tank employing two support acrylic plates (fig. 2k) that hold the obstacle fixed to its initial position while water is being pushed around it.

Free surface perturbations of the moving liquid were analysed using high-speed videography, at a rate of 8000 frames per second. A Photron FASTCAM SA5 camera (fig. 2 l) was used to capture a normal-view angle of the experiment with the axis of the camera aligned with that of the obstacle, as shown in fig. 2. The imaging field of view was set to 105 mm horizontal × 77 mm vertical, which produced a spatial resolution (distance between image pixels) of 0.104 mm. For optimised imaging, an array of high-power LEDs (fig. 2m) and a light diffuser (fig. 2n) are located behind the water tank to provide back-lighting for the recordings. The synchronisation of the LEDs, the triggering of the solenoid valve and the activation of the camera recording is controlled through an Arduino based circuit. The water used in the
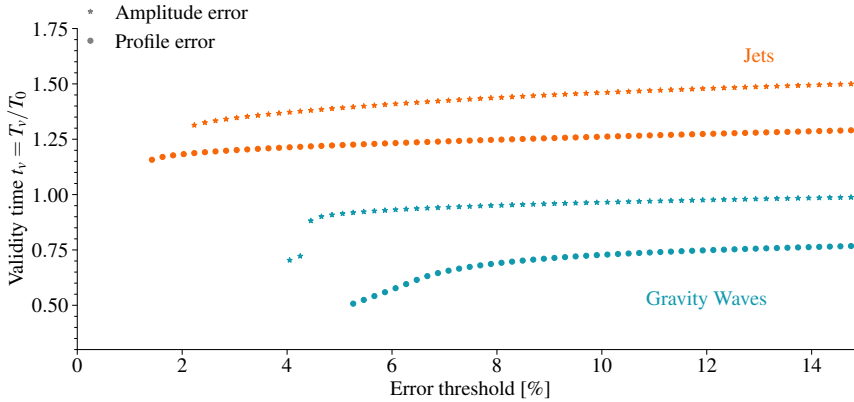
Figure 3: Change of validity times of predictions for perturbation amplitude (stars) and surface profile (circles) for different error thresholds. Results corresponding to experiments that show Jets and Gravity Waves have been displayed in Orange and Blue respectively.

experiments is coloured with food dye to provide high contrast against the illuminated background. An edge-tracking algorithm that relies on the change of light intensity between the fluid and the illuminated background is used to analyse the motion of the liquid and the development of surface perturbations.

The water tank had a lateral depth of 4 cm, a frontal width of 12 cm, and a height of 25 cm (see red labels in fig. 2). A range of cylinders with diameters of 5-15 mm was investigated. This resulted in lateral aspect ratios (lateral window depth to cylinder diameter) ranging between 2.7 to 8, and frontal aspect ratios (frontal window width to obstacle diameter) of 8 to 24. These aspect ratios were sufficient to ensure that end effects due to the walls were mitigated.

2. Analysis of validity time

The validity time t_v was defined in Section 4.2 of the main article to be the time at which the median of the error distribution (be it an amplitude error $E_{\delta\eta}$ or a profile error E_η) surpasses a certain predefined threshold, which was arbitrarily selected to be 10%. Here, we analyse the influence of this threshold on t_v for each type of error.

Figure 3 shows how t_v varies as a function of various error thresholds. Validity times for jets and gravity waves experiments are displayed in orange and cyan respectively. Also, the two type of error defined in Section 4.2 of the main article are presented with different markers.This figure, therefore, indicates which tolerance in prediction error should be utilised when a given validity time is required by a particular application. For example if one require predicting the amplitude (star markers) of jets (orange curves) until at least $t_v = 1.30$, we can expect a maximum amplitude prediction error $E_{\Delta eta}$ of 3%.

For all scenarios, the validity time initially increases as the error threshold increases, before reaching an approximately constant value. We also note that the validity time is greater when predicting the amplitude of the perturbation, compared to that of predicting the surface profile. The profile error for the gravity wave cases has the least validity times across all error thresholds but also reaches its approximately constant value at a larger error threshold as compared to the other cases, this being at roughly 10%. Hence it seems prudent to use this error threshold to determine the critical validity time for all cases, which is what we have done in fig. 9 of the main text. It is also important to stress that the prediction error increases dramatically once this critical validity time is exceeded, even by a small amount. For example, the amplitude error for gravity waves is 5% at $t_v^* \approx 0.95$, 10% at $t_v^* \approx 0.96$, and 15% at $t_v^* \approx 0.98$.